Migration by the Kirchhoff, slant stack, and Gaussian beam methods

Dave Hale

ABSTRACT

Gaussian beam migration offers features that are unmatched by any other single depth migration method. Unfortunately, computer algorithms for Gaussian beam migration are more complicated and difficult to understand than those for most other methods.

One way to simplify Gaussian beam migration is to understand how it is related to other methods that may be more familiar. In particular, Gaussian beam migration is similar to Kirchhoff integral migration. It is also similar to the phase-shift (or slant stack) migration method. In a sense, the Gaussian beam approach to depth migration is to combine the best of these more familiar methods to obtain an efficient, robust, and flexible method for seismic imaging.

INTRODUCTION

Computer programs for Gaussian beam migration tend to be more complicated than those for migration via Kirchhoff, finite-difference, or Fourier transform methods. The software development effort required to implement Gaussian beam migration is substantial, and it is difficult to know whether or not the effort is worthwhile unless you have already made it. Or unless someone else has.

Fortunately, enough research on Gaussian beam migration has recently been published and presented that newcomers to the method (like me) should expect to be rewarded for the time and money invested in understanding and implementing it. In particular, work by Costa, et al. (1989), Lazaratos and Harris (1990), and Hill (1990, 1991) suggests that Gaussian beam migration provides desirable features that are not available with any other single method commonly used today. Among these features are computational efficiency, robustness with respect to ray caustics and shadows, the ability to image reflector dips greater than 90 degrees with turning waves, and

straightforward extensions for migration of non-zero-offset sections and 3-D seismic data. Table 1 provides a brief comparison of several depth migration methods, with respect to these features.

Method	Domain	Efficiency	Robustness	TW?	NZO?
Reverse-time	(t, x, z)	Poor	Good	Yes	No
Finite-difference	(ω, x, z)	Good	Good	No	No
Kirchhoff	(t, x, z)	Good	Poor	Yes	Yes
Slant stack	(τ, p_x, x, z)	Good	Poor	Yes	Yes
Gaussian beam	(τ, p_x, x, z)	Good+	Good	Yes	Yes

Table 1. A subjective comparision of depth migration methods. TW and NZO denote abilities to handle turning waves and non-zero-offset (constant-offset) sections, respectively.

This paper is an introduction to Gaussian beam migration, targeted for readers who are already familiar with migration methods commonly used today, who can appreciate analogies drawn between Gaussian beam migration and more familiar methods. In particular, Gaussian beam migration is shown here to lie somewhere between the Kirchhoff and slant stack migration methods. Slant stack migration, while perhaps the least familiar method listed in Table 1, is shown below to be a variant of the well-known phase-shift (Gazdag, 1978) method.

This paper is not intended to be a substitute for Hill's (1990) paper, which contains several figures and examples that are particularly useful for understanding Gaussian beam migration. Also, this paper does not introduce curvilinear, ray-centered coordinates and their use in Gaussian beam migration, not because these subjects are intuitive or irrelevant, but rather because they have been well presented by others (e.g., Červený et al., 1982). Here, only Cartesian coordinates are used.

Parts of this paper are intended to clarify some parts of Hill's (1990) paper that I found difficult to follow, such as equations (23) through (27) of that paper. Also, this paper derives equations, analogous to Hill's equations (34a) and (34b), for two key sampling parameters that must be computed in Gaussian beam migration.

KIRCHHOFF MIGRATION

Migration in this paper will be discussed in the context of the simplest 2-D, acoustic, constant-density wave equation:

$$\frac{\partial^2 w}{\partial x^2} + \frac{\partial^2 w}{\partial z^2} - \frac{1}{v^2}\frac{\partial^2 w}{\partial t^2} = 0, \tag{1}$$

where $w = w(t, x, z)$ denotes a pressure wavefield, a function of time t, horizontal distance x, and depth z. For migration of zero-offset (stacked) seismic data, based on the exploding reflectors principle (e.g., Claerbout, 1985), the velocity $v = v(x, z)$ in

this equation must be replaced with half-velocity $v/2$. For simplicity, I will assume that v in equation (1) has already been halved.

The Kirchhoff integral method of poststack migration (e.g., Schneider, 1978) can be summarized by the simple equation:

$$g(x,z) = \int dx' \, A(x',x,z) f[t = t(x',x,z), x'], \tag{2}$$

where $g(x,z)$ denotes the subsurface image, and $f(t,x)$ denotes the seismic data recorded at the surface $z = 0$.

The functions $t(x',x,z)$ and $A(x',x,z)$ represent the traveltime and amplitude of a seismic wave that travels from the point $(x', z = 0)$ to the point (x,z). In actual implementations of Kirchhoff migration, some additional filtering of the seismic data $f(t,x)$ must be performed; this filtering is not relevant here and has been omitted in equation (2).

Computations implied by equation (2) can be performed in several ways, depending on the order in which one loops through the variables x', x, and z. Perhaps the most efficient implementation is

Kirchhoff migration:

```
for all points (x,z) {
        g(x,z) = 0
}

for all x' (all seismic traces) {
        for all points (x,z) {
                compute t(x',x,z) and A(x',x,z)
                accumulate contribution to g(x,z) of f(t,x')
        }
}
```

The most difficult part of this algorithm is the accurate and efficient computation of the time and amplitude functions $t(x',x,z)$ and $A(x',x,z)$. This problem is difficult, in part, because these functions may be multi-valued; i.e., more than one seismic wave may arrive at the surface location $(x', z = 0)$ from the same subsurface point (x,z).

This problem is illustrated in Figure 1, which shows the contribution to the migrated image of a single (synthetic) seismic trace "recorded" at surface location $x' = 5\,\text{km}$. The velocity function $v(x,z)$ used in this example has a low-velocity zone centered at horizontal distance $x = 4\,\text{km}$ and depth $z = 1.5\,\text{km}$, embedded in a linearly increasing velocity function $v(x,z) = 1.5 + 0.6z$. Rays traced from the surface location x' are superimposed on the image to highlight the multiple wavefronts

at points in the lower left corner of the image. Rays that intersect at subsurface locations (x, z) imply multi-valued functions $t(x', x, z)$ and $A(x', x, z)$.

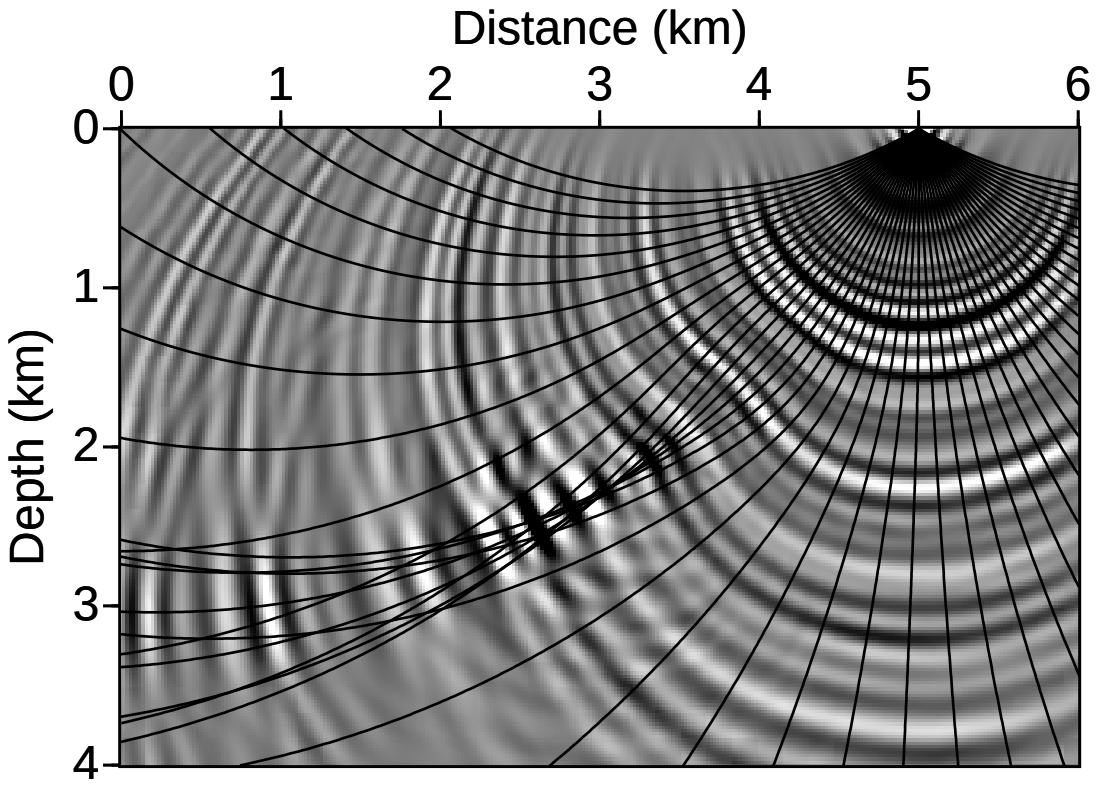

FIG. 1. Contribution of one (synthetic) seismic trace in depth migration. Note (1) the complicated behavior in the lower left corner caused by a low-velocity zone, and (2) that one trace has contributed to almost every point in this subsurface image. In Kirchhoff migration, the complete image is obtained by summing the contributions from all traces.

Ray tracing, such as that illustrated in Figure 1, is often used to compute the functions $t(x', x, z)$ and $A(x', x, z)$. In this example, many of the rays traced from the surface location $x' = 5\,\text{km}$ pass through or near the low-velocity lens and cross in the lower left corner of the model. Asymptotic (WKBJ, high-frequency) ray theory erroneously yields infinite amplitudes where rays cross. Even if the amplitude factor A is omitted from equation (2), it is difficult and computationally expensive to find all of the rays and their corresponding traveltimes t between two points (x, z) and $(x', z = 0)$.

A recent and popular alternative to ray tracing is the direct solution of a non-linear partial differential equation (the eikonal equation) for the traveltime function t (e.g., Vidale, 1988; Van Trier and Symes, 1991). This method and other similar alternatives to ray tracing yield only the shortest traveltime t between any two points

(x, z) and $(x', z = 0)$. Such methods fail to account for the multiple arrivals in the lower left corner of Figure 1.

The problems caused by multi-valued time and amplitude functions (and infinite amplitudes) tend to make Kirchhoff migration less robust in handling lateral velocity variations than the other methods listed in Table 1. In fact, a Gaussian beam method was used to compute the single-trace contribution shown in Figure 1. I did not attempt to reproduce this result with a Kirchhoff depth migration, primarily because of the computational difficulties described above.

The computational cost of Kirchhoff migration is easy to estimate, given the algorithm outlined above. The cost is proportional to the number of traces (number of x') times the number of subsurface points (x, z) to be imaged. Assuming that the number of samples in each dimension (time or space) is proportional to, say, the number of time samples N in each seismic trace, the cost of Kirchhoff migration goes as N^3. This estimate is based on the assumption that $t(x', x, z)$ and $A(x', x, z)$ can be computed in constant time for any given x', x, and z. As shown below, a cost proportional to N^3 is typical of depth migration methods.

SLANT STACK MIGRATION

The second depth migration method considered in this paper is one that, to my knowledge, is never used. It is useful only because it is similar to migration methods that are used, and because it represents one extreme in a spectrum of migration methods that includes Gaussian beam migration.

Phase-shift migration

First, recall Gazdag's (1978; Claerbout, 1985, 30–33) phase-shift method for depth extrapolation of a seismic wavefield in the frequency-wavenumber (ω, k_x) domain:

$$W(\omega, k_x, z) = W(\omega, k_x, z = 0)\, A(k_x/\omega, z)\, e^{-i\omega \int_0^z d\zeta \frac{\cos\theta(k_x/\omega, \zeta)}{v(\zeta)}}, \tag{3}$$

where $\theta(p_x, z)$ is the angle defined by

$$\sin\theta(p_x, z) = v(z)p_x,$$

and

$$A(p_x, z) = \left[\frac{v(z)\cos\theta_0}{v_0\cos\theta(p_x, z)}\right]^{1/2}. \tag{4}$$

Equation (3) is the WKBJ solution (e.g., Aki and Richards, 1980, 416) to the differential equation,

$$\frac{d^2W}{dz^2} + \left[\frac{\omega^2}{v^2(z)} - k_x^2\right] W = 0,$$

which is the wave equation (1), expressed in the frequency-wavenumber domain. Although velocity $v(z)$ is here restricted to be a function of depth z only, this limitation will be removed below.

The angle $\theta(p_x, z)$ defined above is the propagation angle at depth z of a plane wave that emerges at the earth's surface with angle θ_0 and velocity v_0 satisfying $\sin\theta_0 = v_0 p_x$.

In phase-shift migration, the amplitude function $A(p_x, z)$ is often omitted, in part because it goes to infinity as z approaches the turning point, that depth where $\theta(p_x, z) = \pm 90$ degrees. This erroneous infinite amplitude is similar to that encountered when performing Kirchhoff migration with WKBJ amplitudes determined by ray tracing.

For migration of zero-offset seismic data $f(t, x)$, we identify $W(\omega, k_x, z = 0)$ as the Fourier transformed data $F(\omega, k_x)$. Inverse Fourier transform equation (3) from wavenumber k_x to distance x,

$$W(\omega, x, z) = \frac{1}{2\pi} \int dk_x \, A(k_x/\omega, z) \, e^{-i\omega \int_0^z d\zeta \, \frac{\cos\theta(k_x/\omega, \zeta)}{v(\zeta)} + ik_x x} \, F(\omega, k_x), \tag{5}$$

and then evaluate the inverse Fourier transform from frequency ω to time t at $t = 0$ to obtain the subsurface image

$$\begin{aligned} g(x, z) &= \frac{1}{2\pi} \int d\omega \, e^{-i\omega t = 0} \, W(\omega, x, z) \\ &= \frac{1}{4\pi^2} \int d\omega \int dk_x \, A(k_x/\omega, z) \, e^{-i\omega \int_0^z d\zeta \, \frac{\cos\theta(k_x/\omega, \zeta)}{v(\zeta)} + ik_x x} \, F(\omega, k_x). \end{aligned} \tag{6}$$

Equation (6) concisely summarizes the phase-shift migration method.

From wavenumber k_x to reflection slope p_x

The ratio $p_x = k_x/\omega$ that appears in phase-shift migration corresponds to the slope of a reflection recorded in the seismic data $f(t, x)$. Equation (5) implies that each reflection slope p_x can be extrapolated in depth independently. This motivates a change in integration variable from k_x to p_x:

$$\begin{aligned} W(\omega, x, z) &= \frac{1}{2\pi} \int dp_x \, |\omega| A(p_x, z) e^{-i\omega \int_0^z d\zeta \, \frac{\cos\theta(p_x, \zeta)}{v(\zeta)} + i\omega p_x x} \, F(\omega, k_x = \omega p_x) \\ &= \int dp_x \, A(p_x, z) e^{-i\omega\tau(p_x, x, z)} B(\omega, p_x), \end{aligned} \tag{7}$$

where

$$B(\omega, p_x) \equiv \frac{|\omega|}{2\pi} F(\omega, k_x = \omega p_x), \tag{8}$$

and

$$\tau(p_x, x, z) \equiv \int_0^z d\zeta \, \frac{\cos\theta(p_x, \zeta)}{v(\zeta)} \; - \; p_x x. \tag{9}$$

With this change of variables, equation (6) becomes

$$g(x,z) = \int dp_x \, A(p_x,z) \, \frac{1}{2\pi} \int d\omega \, e^{-i\omega\tau(p_x,x,z)} \, B(\omega,p_x).$$

Recognizing that the integral over frequency ω is just an inverse Fourier transform, we obtain the following expression for the subsurface image:

$$g(x,z) = \int dp_x \, A(p_x,z) \, b[\tau = \tau(p_x,x,z), p_x]. \tag{10}$$

An appropriate name for equation (10) is *slant stack migration* because the function $b(\tau,p_x)$ is a filtered slant stack of the surface seismic data $f(t,x)$. Specifically,

$$b(\tau,p_x) = \rho(\tau) * \int dx \, f(t = \tau + p_x x, x),$$

where $\rho(\tau)$ is the so-called "rho" filter defined by

$$\rho(\tau) \equiv \frac{1}{2\pi} \int d\omega \, e^{-i\omega\tau} \frac{|\omega|}{2\pi}.$$

To verify this relationship between $b(\tau,p_x)$ and $f(t,x)$, Fourier tranform $b(\tau,p_x)$ to obtain

$$\begin{aligned} B(\omega,p_x) &= \frac{|\omega|}{2\pi} \int d\tau \, e^{i\omega\tau} \int dx \, f(t = \tau + p_x x, x) \\ &= \frac{|\omega|}{2\pi} \int dx \, e^{-i\omega p_x x} \, F(\omega,x) \\ &= \frac{|\omega|}{2\pi} \, F(\omega, k_x = \omega p_x), \end{aligned}$$

which matches the definition of $B(\omega,p_x)$ given by equation (8) above.

Although the derivation of slant stack migration above began with the restriction that velocity varies with depth only, equation (10) can be generalized to account for lateral velocity variations, as suggested by the work of Sinton and Frazer (1982). In the general case of $v = v(x,z)$, the amplitude function A depends on horizontal distance x as well as reflection slope p_x and depth z, and both functions $A(p_x,x,z)$ and $\tau(p_x,x,z)$ are more difficult to compute than for the laterally homogeneous case.

However, as in Kirchhoff migration, these functions can be computed by ray tracing. In particular, the function $\tau(p_x,x,z)$ can be computed by

$$\tau(p_x,x,z) = t(p_x,x,z) - p_x x', \tag{11}$$

where $t(p_x,x,z)$ denotes the time required for a ray to travel from the subsurface point (x,z) to the surface with emergence angle $\theta_0 = \arcsin(v_0 p_x)$. v_0 denotes the velocity at the surface location x' where the ray intersects the surface. Substitution

of the traveltime function $\tau(p_x, x, z)$ defined by equation (11) and a corresponding amplitude function $A(p_x, x, z)$ into equation (10) yields *slant stack depth migration.*

The most straightforward algorithm for slant stack migration is analogous to that for Kirchhoff migration:

Slant stack migration:

compute filtered slant stack $b(\tau, p_x)$ *of seismic data* $f(t, x)$

for all points (x, z) {
    $g(x, z) = 0$
}

for all p_x *(all reflection slopes)* {
    for all points (x, z) {
        compute $\tau(p_x, x, z)$ *and* $A(p_x, x, z)$
        accumulate contribution to $g(x, z)$ *of* $b(\tau, p_x)$
    }
}

As for Kirchhoff migration, the most difficult part of this algorithm is the accurate and efficient computation of the time and amplitude functions $\tau(p_x, x, z)$ and $A(p_x, x, z)$. Again, these functions may be multi-valued. Figure 2 shows the contribution to the migrated image of a single reflection slope p_x, corresponding to an emergence angle of 20 degrees. The velocity function $v(x, z)$ used in this example is the same as that of Figure 1. Rays with the same emergence angle, but different emergence locations, are superimposed on the image. Where rays intersect at a subsurface point (x, z), the functions $\tau(p_x, x, z)$ and $A(p_x, x, z)$ are multi-valued.

Even when velocity varies with depth only, the time (and amplitude) functions may be multi-valued. To see why, simply trace two rays with the same emergence angle, but different emergence locations, backwards into a subsurface in which velocity increases with depth. The rays will intersect after one of them has turned beyond 90 degrees. When velocity varies with depth only, just two times $\tau(p_x, x, z)$ are feasible — one corresponds to the ray that has not yet reached its turning point, and the other corresponds to the turned ray.

Assuming that ray tracing is used to compute the necessary time (and amplitude) functions, the difference between the ray tracing for Kirchhoff depth migration and that for slant stack depth migration is interesting. In Kirchhoff migration, we require the time $t(x', x, z)$, which we may determine by tracing rays with different emergence angles θ_0 backwards from the emergence location x', until we find all of the rays that pass through the subsurface point (x, z). In this approach, given x', x, and z, we

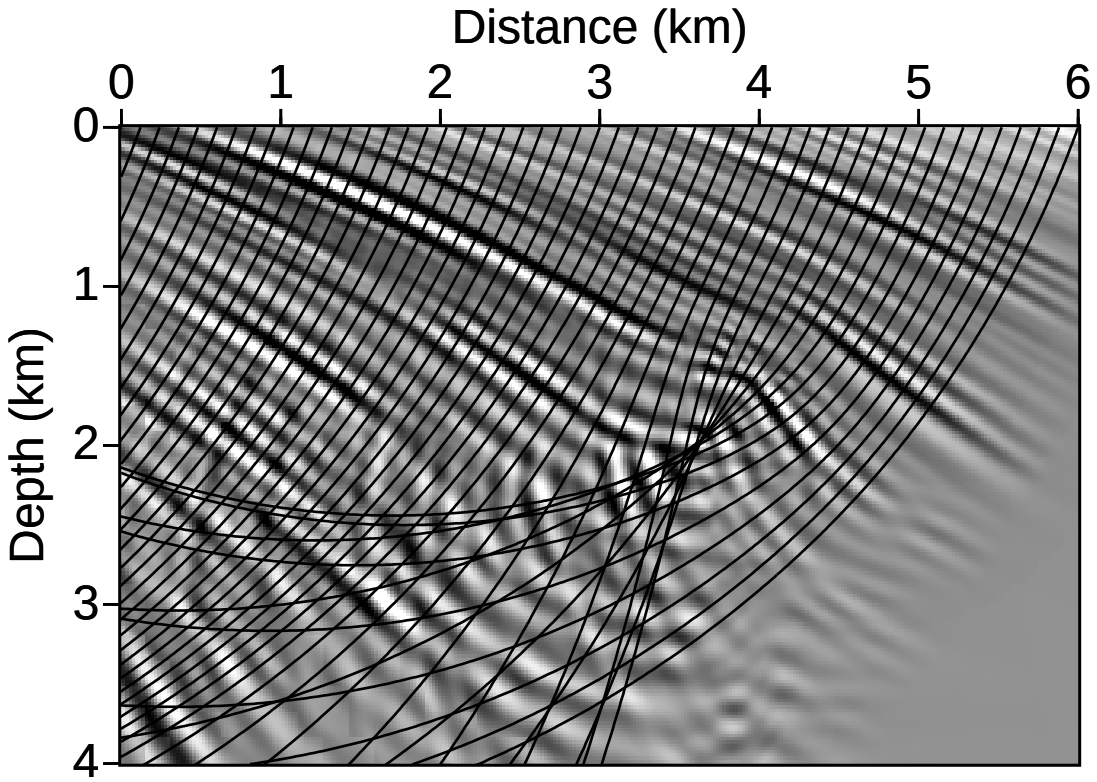

FIG. 2. Contribution of one reflection slope p_x in depth migration. Note (1) the complicated behavior in the lower left corner caused by a low-velocity zone, and (2) that one slope p_x contributes to almost every point in the subsurface image. In slant stack migration, the complete image is obtained by summing the contributions from all reflection slopes.

search for the appropriate emergence angles θ_0, or equivalently, reflection slopes p_x. In slant stack migration, we require the time $\tau(p_x, x, z)$. Given p_x, x, and z, we search for the emergence locations x' required by equation (11).

In a computer implementation of slant stack migration, we must convert the integral over reflection slope p_x in equation (10) to a sum, which implies that we must determine how finely to sample p_x. The definition of $p_x = k_x/\omega$ suggests that we choose $\Delta p_x = \Delta k_x/\omega$, where Δk_x is the sampling of wavenumber k_x we would use in phase-shift migration. To avoid aliasing, we would choose $\Delta k_x = 2\pi/X$, where X denotes the horizontal width of the seismic data to be migrated. To implement equation (10) we must use a sampling interval p_x that is independent of frequency. Therefore, we choose

$$\Delta p_x = \frac{2\pi}{\omega_h X}, \tag{12}$$

to avoid aliasing frequencies less than the highest frequency of interest, ω_h.

Because of the similarities between the algorithms for Kirchhoff and slant stack migrations, it is easy to verify that slant stack migration, like Kirchhoff migration, has a computational cost proportional to N^3, where N is again the number of time samples. The number of slopes p_x that must be imaged is, from equation (12), proportional to the number of seismic traces, which tends to grow in proportion to N. The cost of computing the filtered slant stacks $b(\tau, p_x)$ via FFTs [equation (8)] is proportional to $N^2 \log N$ and is, therefore, likely to be a negligible part of the total cost proportional to N^3.

Given their similar computational costs, one might wonder why slant stack migration is used less often than Kirchhoff migration. Perhaps the best explanation is that *slant stack migration is less straightforward and no better than Kirchhoff migration.* Slant stack migration is certainly no more robust than Kirchhoff migration. Because of the difficulties in computing the multi-valued time and amplitude functions $\tau(p_x, x, z)$ and $A(p_x, x, z)$, the single-slope contribution shown in Figure 2 was computed via a robust Gaussian beam algorithm, rather than the slant stack algorithm outlined above.

One way to obtain a robust depth migration would be to combine the Kirchhoff and slant stack methods, blending the single-trace and single-slope contributions together to obtain the image at any given subsurface point (x, z). For any (x, z), we might choose the blending weights to emphasize the contribution that is most accurate. For example, where the Kirchhoff method implies infinite amplitude at a point (x, z), we would use the slant stack method to compute the contribution at that point. This blending approach is analogous to that proposed for seismic modeling by Chapman and Drummond (1982). That approach, which is based on Maslov asymptotic theory, depends on the fact (not proven here) that the Kirchhoff and slant stack methods are guaranteed not to fail simultaneously at any point (x, z).

As shown in the following section, Gaussian beams provide another technique for combining the Kirchhoff and slant stack methods to obtain a robust depth migration algorithm.

GAUSSIAN BEAM MIGRATION

Recall that the first step in slant stack migration is the computation of the filtered slant stack $b(\tau, p_x)$ of the seismic data $f(t, x)$ recorded at the surface. This slant stacking decomposes $f(t, x)$ into plane waves, with each reflection slope p_x corresponding to a different plane wave component. In contrast, Kirchhoff migration requires no preliminary decomposition of the seismic data $f(t, x)$; the decomposition into individual seismic traces at unique surface locations x' was performed when the data were recorded.

Gaussian beam migration is similar to slant stack migration, in that it too requires that $f(t, x)$ be decomposed with slant stacking. The difference is that Gaussian beam migration computes many *local slant stacks (beams)*, each computed from small

overlapping subsets of the seismic data. As in slant stack migration, each plane wave component of each subset contributes to the migrated image independently, and all contributions are summed to obtain the complete subsurface image.

Local slant stacks

First, we extract a window of the data $f(t,x)$ by applying a lateral shift and a frequency-dependent Gaussian taper:

$$F_j(\omega,x) \equiv e^{-\frac{1}{2}\left|\frac{\omega}{\omega_l}\right|\frac{x^2}{l^2}}\, F(\omega, x+x_j), \tag{13}$$

where x_j is the center of the Gaussian window, and l is the width (standard deviation) of the Gaussian when frequency $\omega=\omega_l$. It is convenient to choose ω_l to be the lowest frequency of interest, so that l is related to the maximum width of the Gaussian. If we assume a Gaussian amplitude of $1/100$ is negligible, then the width of the data window after Gaussian tapering is approximately $X = 6l\sqrt{|\omega_l/\omega|}$.

The local slant stack of $F_j(\omega,x)$ is defined as in equation (8) by

$$\begin{aligned} B_j(\omega,p_x) &\equiv C\frac{|\omega|}{2\pi}\int dx\, e^{-i\omega p_x x}\, F_j(\omega,x) \\ &= C\frac{|\omega|}{2\pi}\, F_j(\omega, k_x=\omega p_x). \end{aligned} \tag{14}$$

The extra scale factor C in this local slant stack will be determined below to normalize the sum of overlapping Gaussian windows.

Local slant stacks, like the slant stacks of the preceding section, must be adequately sampled in p_x. Using the criterion of equation (12), but with X determined by the width of the Gaussian window, we obtain

$$\Delta p_x = \frac{2\pi}{\omega_h X} = \frac{\pi}{3l\sqrt{|\omega_l\omega_h|}}, \tag{15}$$

which guarantees that frequencies less than the highest frequency of interest ω_h will not be aliased. Although the derivation here of Δp_x is quite different, the result is similar to that in Hill's (1990) equation (34b). The only difference is that Hill has a factor of 4 in the denominator where equation (15) has a factor of 3.

Depth extrapolation

Depth extrapolation of the locally slant stacked (beam-formed) data window can be performed as suggested by equation (7):

$$W_j(\omega,x,z) = \int dp_x\, A_j(p_x,x,z) e^{-i\omega\tau_j(p_x,x,z)} B_j(\omega,p_x). \tag{16}$$

The function $W_j(\omega, x, z)$ is only a part of the complete wavefield, because it is computed for a single Gaussian window of data. The complete wavefield is given by summing up contributions from many overlapping windows of data; i.e.,

$$W(\omega, x, z) = \sum_j W_j(\omega, x, z).$$

The key problem here, as in slant stack migration, is to compute the time and amplitude functions $\tau_j(p_x, x, z)$ and $A_j(p_x, x, z)$. The dynamic ray tracing solution to this problem is:

1. Trace *one* ray, with emergence location x_j and emergence angle $\theta_j = \arcsin[v(x_j, 0)p_x]$.
2. Solve *dynamic ray tracing* equations along the ray for both point and plane-wave sources.
3. Combine solutions for both point and plane-wave sources to obtain *complex-valued* time and amplitude functions $\tau_j(p_x, x, z)$ and $A_j(p_x, x, z)$.

A complete explanation of these three steps requires the introduction of concepts such as curvilinear ray-centered coordinates, which in this paper would be an unnecessary distraction. Hill's (1990) paper summarizes these three steps concisely, and more complete discussions are provided by Červený, et al. (1982) and Červený and Pšenčík (1984).

Were it not for the fact that both $\tau_j(p_x, x, z)$ and $A_j(p_x, x, z)$ are complex-valued, depth extrapolation for local slant stacks would be no more robust than that for the global slant stacks of the previous section. The complex combination of solutions to the dynamic ray tracing equations for both point and plane-wave sources ensures that amplitudes will be well-behaved. In particular, the complex-valued amplitude function $A_j(p_x, x, z)$ never goes to infinity, unlike the WKBJ amplitude functions for Kirchhoff, phase-shift, or slant-stack migrations.

Another important feature of the complex times and amplitudes computed by dynamic ray tracing for Gaussian beams is that they are single-valued, unlike those computed for Kirchhoff or slant stack migration.

Matching the surface seismic data

As in slant stack migration, we must ensure that the seismic wavefield at the surface $W(\omega, x, z = 0)$ matches the seismic data $F(\omega, x)$. To this end, we arrange for the complex-valued time and amplitude functions evaluated at $z = 0$ to be

$$\begin{aligned} \tau_j(p_x, x, z = 0) &= p_x(x - x_j) - \frac{i}{2}\frac{\mathrm{sgn}(\omega)}{|\omega_l|}\frac{(x - x_j)^2}{l^2} \\ A_j(p_x, x, z = 0) &= 1. \end{aligned} \tag{17}$$

The choice of the Gaussian width l determines the weighting of the point source and plane-wave source solutions to the dynamic ray tracing equations. Specifically, a tiny l corresponds to a point source, and a huge l corresponds to a plane-wave source.

Inserting the times and amplitudes given by equations (17) into the expression for the seismic wavefield given by equation (16), we obtain

$$\begin{aligned} W_j(\omega,x,z=0) &= e^{-\frac{1}{2}\left|\frac{\omega}{\omega_l}\right|\frac{(x-x_j)^2}{l^2}} \int dp_x\, e^{i\omega p_x(x-x_j)}\, B_j(\omega,p_x) \\ &= C\, e^{-\frac{1}{2}\left|\frac{\omega}{\omega_l}\right|\frac{(x-x_j)^2}{l^2}}\, F_j(\omega,x-x_j) \\ &= C\, e^{-\left|\frac{\omega}{\omega_l}\right|\frac{(x-x_j)^2}{l^2}}\, F(\omega,x). \end{aligned}$$

The complete wavefield at the surface is

$$\begin{aligned} W(\omega,x,z=0) &= \sum_j W_j(\omega,x,z=0) \\ &= F(\omega,x)\, C \sum_j e^{-\left|\frac{\omega}{\omega_l}\right|\frac{(x-x_j)^2}{l^2}} \\ &\approx F(\omega,x). \end{aligned}$$

Hill (1990) showed that the error in the last approximation is about 1 percent if

$$\begin{aligned} x_j &= j\Delta \\ \Delta &< \left|\frac{2\omega_l}{\omega}\right|^{1/2} l \\ C &= \left|\frac{\omega}{\pi\omega_l}\right|^{1/2} \frac{\Delta}{l}. \end{aligned} \tag{18}$$

Here, Δ is the spacing between the beam center location x_j, the centers of the overlapping Gaussian windows. In order for this spacing to be independent of frequency, we choose

$$\Delta = \left|\frac{2\omega_l}{\omega_h}\right|^{1/2} l, \tag{19}$$

where ω_h is again the highest frequency of interest. The frequency-dependent scale factor C given by equation (18) is most conveniently applied when filtering the local slant stacks, as suggested by equation (14).

Hill's (1990) recommended value for Δ is similar to that given above by equation (19). The only difference is that Hill's equation (34a) has a factor 2 where equation (19) has a factor $\sqrt{2}$. Thus, Hill recommends a somewhat larger spacing between beam center locations and a somewhat finer sampling of p_x [recall equation (15)] than are derived here. The differences between the values for Δ and p_x in this paper

and those recommended by Hill are likely due to the application of a Gaussian taper in equation (13) above. A different, non-Gaussian taper is implied by Hill's equation (27).

The subsurface image

Given equation (16), which describes one contribution $W_j(\omega, x, z)$ to the complete seismic wavefield, we need only sum these contributions and integrate over frequency ω, as in slant stack migration, to obtain the subsurface image. Specifically, the complete image is obtained by

$$g(x,z) = \sum_j g_j(x,z),$$

where

$$\begin{aligned} g_j(x,z) &= \frac{1}{2\pi}\int d\omega\, W_j(\omega,x,z) \\ &= \int dp_x\, A_j(p_x,x,z)\,\frac{1}{2\pi}\int d\omega\, e^{-i\omega\tau_j(p_x,x,z)} B_j(\omega,p_x). \end{aligned} \tag{20}$$

If the time and amplitude functions τ_j and A_j in equation (20) were real-valued, then it would be straightforward to identify the integral over frequency as an inverse Fourier transform, and to obtain an equation analogous to equation (10) for slant stack migration. Complex-valued τ_j and A_j make Gaussian beam amplitudes well behaved, but they complicate our implementation of equation (20). In particular, we require that $g_j(x,z)$ be real-valued, which means that we must preserve conjugate symmetry in the frequency domain. Specifically, the sign of the imaginary parts of τ_j and A_j must depend on the sign of ω.

To see how to implement equation (20), we should express τ_j and A_j in terms of their real and imaginary parts:

$$\begin{aligned} \tau &= \tau_R + i\,\mathrm{sgn}(\omega)\tau_I \\ A &= A_R + i\,\mathrm{sgn}(\omega)A_I. \end{aligned}$$

Remember that τ_R, τ_I, A_R, and A_I are all functions of the beam center location x_j, the reflection slope p_x, and the subsurface image coordinates (x,z), even though this dependence has not been stated explicitly in order to simplify notation below. In terms of these real and imaginary parts, equation (20) may be written more precisely as

$$g_j(x,z) = \int dp_x\,\frac{1}{2\pi}\int d\omega\,[A_r + i\,\mathrm{sgn}(\omega)A_I]\,e^{-i\omega\tau_R+|\omega|\tau_I} B_j(\omega,p_x). \tag{21}$$

Note that, to avoid exponential growth of the integrand, we require $\tau_I \le 0$, which is consistent with equations (17).

Straightforward implementation of equation (21) would require numerous costly integrations over frequency ω. Therefore, we seek an equivalent time-domain expression by first defining

$$\tilde{B}(\omega, \tau_I) \equiv e^{|\omega|\tau_I} B_j(\omega, p_x), \tag{22}$$

followed by its time-domain equivalent

$$\tilde{b}(\tau_R, \tau_I) = \frac{1}{2\pi} \int d\omega \, e^{-i\omega\tau_R} \tilde{B}(\omega, \tau_I). \tag{23}$$

Both $\tilde{B}$ and $\tilde{b}$ are functions of beam center location x_j and reflection slope p_x, although this dependence has been suppressed to simplify notation. To account for the complex amplitude function A in equation (21), recall that multiplication by $-i\text{sgn}(\omega)$ in the frequency domain is equivalent to a Hilbert transform in the time domain. Therefore, equation (21) becomes

$$g_j(x, z) = \int dp_x \left[A_R \tilde{b}(\tau_R, \tau_I) - A_I \tilde{b}_H(\tau_R, \tau_I) \right], \tag{24}$$

where $\tilde{b}_H$ denotes the Hilbert transform of $\tilde{b}$. Equation (24) is similar to equation (10) for slant stack migration; the differences are due entirely to the use of complex time and amplitude functions in Gaussian beam migration.

Algorithm and cost

Equation (24), with all of the steps necessary to evaluate the integrand, accounts for most of the computational effort in Gaussian beam migration. It describes the contribution to the subsurface image of one Gaussian-tapered window of seismic data. The complete image is obtained by summing all such contributions, as in the following algorithm for Gaussian beam migration:

Gaussian beam migration:

for all points (x, z) {
    $g(x, z) = 0$
}

for all $x_j = j\Delta$ *(all beam center locations)* {
    compute $f_j(t, x)$ *by shifting and tapering data* $f(t, x)$
    compute filtered slant stack $b_j(\tau, p_x)$ *of* $f_j(t, x)$
    for all p_x *(all reflection slopes)* {
        for all points (x, z) *within beam* {
            compute complex-valued $\tau_j(p_x, x, z)$ *and* $A_j(p_x, x, z)$
            accumulate contribution to $g(x, z)$ *of* $b_j(\tau, p_x)$
        }
    }
}

This algorithm for Gaussian beam migration is similar to both the Kirchhoff and slant stack migration algorithms. One obvious difference is that Gaussian beam migration has two loops outside the innermost loop over subsurface image coordinates (x, z), whereas the Kirchhoff and slant stack methods have only one. This observation might lead us to suspect that Gaussian beam migration is more costly than either Kirchhoff or slant-stack migration. If the cost of the latter algorithms is proportional to N^3, is the cost of Gaussian beam migration proportional to N^4?

The answer to this question is that although the computational cost of Gaussian beam migration is somewhat difficult to estimate, it is certainly no greater than N^3. The cost of the outer two loops is proportional to the number of beam center locations x_j times the number of reflection slopes p_j, which is proportional to N, not N^2. This is because the spacing between beam center locations Δ is proportional to the beam width l at the surface, whereas the sampling interval Δp_x is inversely proportional to l. [Recall equations (15) and (19).] For large beam widths, we have many reflection slopes but few Gaussian windows of data to migrate. For small beam widths, we have more Gaussian windows, but fewer reflection slopes to migrate. Therefore, the cost of the outer two loops in Gaussian beam migration is proportional to N.

Consider now the cost of the innermost loop over subsurface image coordinates (x, z). For Kirchhoff and slant-stack migration, the cost of the innermost loop is proportional to N^2. Each trace or each reflection slope contributes to almost every sample in the subsurface image, a computational grid that tends to grow as the square of the number of time samples N in a seismic trace. For Gaussian beam migration, the cost of the innermost loop is proportional to N times the width of a Gaussian beam. Depending on the beam width, this product may be significantly less than the comparable product for Kirchhoff or slant-stack migration, which accounts for the "Good+" efficiency rating of Gaussian beam migration in Table 1.

Figure 3 illustrates the contribution of one beam in the innermost loop of Gaussian beam depth migration. Although the width of the beam grows with distance from the surface in this example, the area within the beam is less than the area affected by a single trace in Kirchhoff migration or a single reflection slope in slant stack migration.

The difficulty in estimating the cost of Gaussian beam migration lies in the difficulty in estimating the width of the beam, for a given width l at the surface. At great distances from the surface, the beam width becomes asymptotically proportional to N. The important issue is how quickly the beam width approaches its asymptotic value. However, even in the worst case, where the beam widens rapidly away from the surface, the computational cost of the innermost loop is proportional to N^2. Therefore, the total cost of Gaussian beam migration grows at a rate no greater than N^3.

Note that the wavefronts in the Gaussian beam of Figure 3 are simple, because dynamic ray tracing for a single ray was used to compute the complex-valued time and amplitude functions that describe the beam. Dynamic ray tracing makes these functions single-valued, so that the contribution of a single Gaussian beam to the

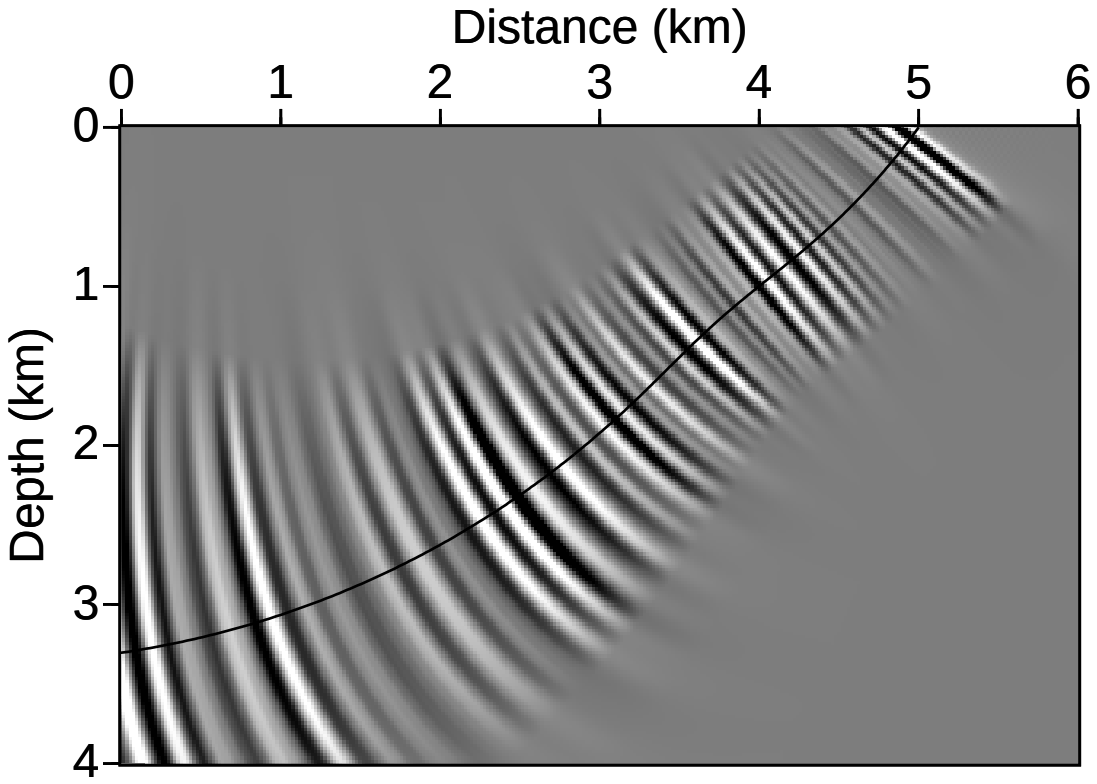

FIG. 3. Contribution of one Gaussian beam in depth migration. Note (1) the distortion of the beam caused by a low-velocity zone, and (2) that one beam contributes to fewer subsurface image points than one trace in Kirchhoff migration or one reflection slope in slant stack migration. The complete image is obtained by accumulating many such contributions.

migrated image is simpler to compute than that of a single trace in Kirchhoff migration or of a single reflection slope in slant stack migration.

CONCLUSION

Kirchhoff integral migration images each seismic trace independently. Because a single trace is very localized in space, it contributes significant energy at all wave propagation angles to the subsurface image. For a single trace, more than one propagation angle can contribute to a single image point.

Slant stack migration images each reflection slope independently. A single reflection slope contributes to a narrow range of propagation angles, but each slope consists of all traces, resulting in extremely wide wavefronts that extend from one end of the seismic section to the other. For a single reflection slope, more than one trace can contribute to a single image point.

Gaussian beam migration lies somewhere between the Kirchhoff and slant stack methods. Instead of migrating one trace at a time for all reflection slopes (as in Kirchhoff migration) or one reflection slope for all traces (as in slant stack migration), Gaussian beam migration independently images each reflection slope in overlapping, Gaussian-tapered subsets of traces. The innermost loop of Gaussian beam migration is the accumulation of a relatively narrow beam that represents a narrow range of propagation angles. Each beam contributes no more than once to each image point.

ACKNOWLEDGMENTS

Support for this work was provided by the members of the Consortium Project on Seismic Inverse Methods for Complex Structures at the Center for Wave Phenomena, Colorado School of Mines.

REFERENCES

Aki, K., and Richards, P. G., 1980, Quantitative seismology, theory and methods: W. H. Freeman and Company.

Červený, V., Popov, M. M., and Pšenčík, I., 1982, Computation of wave fields in inhomogeneous media — Gaussian beam approach: Geophys. J. R. astr. Soc., **70**, 109–128.

Červený, V., and Pšenčík, I., 1984, Gaussian beams in elastic 2-D laterally varying layered structures: Geophys. J. R. astr. Soc., **78**, 65–91.

Chapman, C. H., and Drummond, R., 1982, Body-wave seismograms in inhomogeneous media using Maslov asymptotic theory: Bull. Seis. Soc. Am., **72**, no. 6, S277–S317.

Claerbout, J. F., 1985, Imaging the Earth's interior: Blackwell Scientific Publications.

Costa, C. a., Raz, S., and Kosloff, D., 1989, Gaussian beam migration: Presented at the 59th Ann. Internat. Mtg. Soc. Expl. Geophys., Expanded Abstracts, 1169–1171.

Gazdag, J., 1978, Wave equation migration with the phase-shift method: Geophysics, **43**, 1342–1351.

Hill, N. R., 1990, Gaussian beam migration: Geophysics, **55**, 1416–1428.

Hill, N. R., Watson, T. H., Hassler, M. H., and Sisemore, L. K., 1991, Salt-flank imaging using Gaussian beam migration: Presented at the 61st Ann. Internat. Mtg. Soc. Expl. Geophys., Expanded Abstracts, 1178–1180.

Lazaratos, S. K., and Harris, J. M., 1990, Radon transform / Gaussian beam migration: Presented at the 60th Ann. Internat. Mtg. Soc. Expl. Geophys., Expanded Abstracts, 1314–1317.

Schneider, W. A., 1978, Integral formulation for migration in two and three dimensions: Geophysics, **43**, 49–76.

Sinton, J. B., and Frazer, L. N., 1981, A method for the computation of finite frequency body wave synthetic seismograms in laterally varying media: Geophys. J., **71**, 35–55.

van Trier, J., and Symes, W. W., 1991, Upwind finite-difference calculation of traveltimes: Geophysics, **56**, 812–821.

Vidale, J., 1988, Finite-difference calculation of traveltimes: Bull. Seis. Soc. Am. **78**, no. 6, 2062–2076.